Обзор ArXiv/astro-ph, 16-27 марта 2020

От Сильченко О.К.

ArXiv: 2003.06429

ABSORPTION LINE ABUNDANCES IN THE SMC-LIKE GALAXY UGC 5282: EVIDENCE OF ISM DILUTION FROM INFLOWS ON KPC SCALES *

DAVID V. BOWEN,[1] TODD M. TRIPP,[2] EDWARD B. JENKINS,[1] MAX PETTINI,[3] DORON CHELOUCHE,[4] RENYUE CEN,[1] AND DONALD G. YORK[5]

[1]*Princeton University Observatory, Ivy Lane, Princeton, NJ 08544.*
[2]*Dept. of Astronomy, University of Massachusetts, 710 North Pleasant Street, Amherst, MA 01003.*
[3]*Institute of Astronomy, University of Cambridge, Madingley Road, Cambridge, CB3 0EZ, UK.*
[4]*Dept. of Physics, University of Haifa, Mount Carmel, Haifa 31905, Israel.*
[5]*Dept. of Astronomy and Astrophysics, University of Chicago, Enrico Fermi Institute, 5640 South Ellis Avenue, Chicago, IL 60637.*

(Received 21 September 2019; Accepted 9 March 2020)

ABSTRACT

We present an HST *Cosmic Origins Spectrograph* (COS) spectrum of the QSO SDSS J095109.12+330745.8 ($z_{\rm em}$ = 0.645) whose sightline passes through the SMC-like dwarf galaxy UGC 5282 (M_B = −16.0, cz = 1577 km s^{-1}), 1.2 kpc in projection from the central H II region of the galaxy. Damped Lyα (DLA) absorption is detected at the redshift of UGC 5282 with $\log[N({\rm H\ I})\ {\rm cm}^{-2}] = 20.89^{+0.12}_{-0.21}$. Analysis of the accompanying S II, P II and O I metal lines yields a neutral gas metallicity $Z_{\rm H\,I}$ of [S/H] $\simeq$ [P/H] = −0.80 ± 0.24. The metallicity of ionized gas from the central H II region, $Z_{\rm H\,II}$, measured from its emission lines is [O/H]= −0.37 ± 0.10, a difference of +0.43 ± 0.26 from $Z_{\rm H\,I}$. This difference δ is consistent with that seen towards H II regions in other star-forming galaxies and supports the idea that ionized gas near star forming regions show systematically higher metallicities than exist in the rest of a galaxy's neutral interstellar medium (ISM). The positive values of δ found in UGC 5282 (and the other star forming galaxies) is likely due to infalling low metallicity gas from the intergalactic medium which mixes with the galaxy's ISM on kpc scales. This model is also consistent with broad Lyα emission detected at the bottom of the DLA absorption, offset by $\sim$ 125 km s^{-1} from the absorption velocity. Models of galaxy evolution which attempt to replicate population characteristics, such as the mass-metallicity relation, may need to start with a galaxy metallicity represented by $Z_{\rm H\,I}$ rather than that measured

Карлик, похожий на ММО?

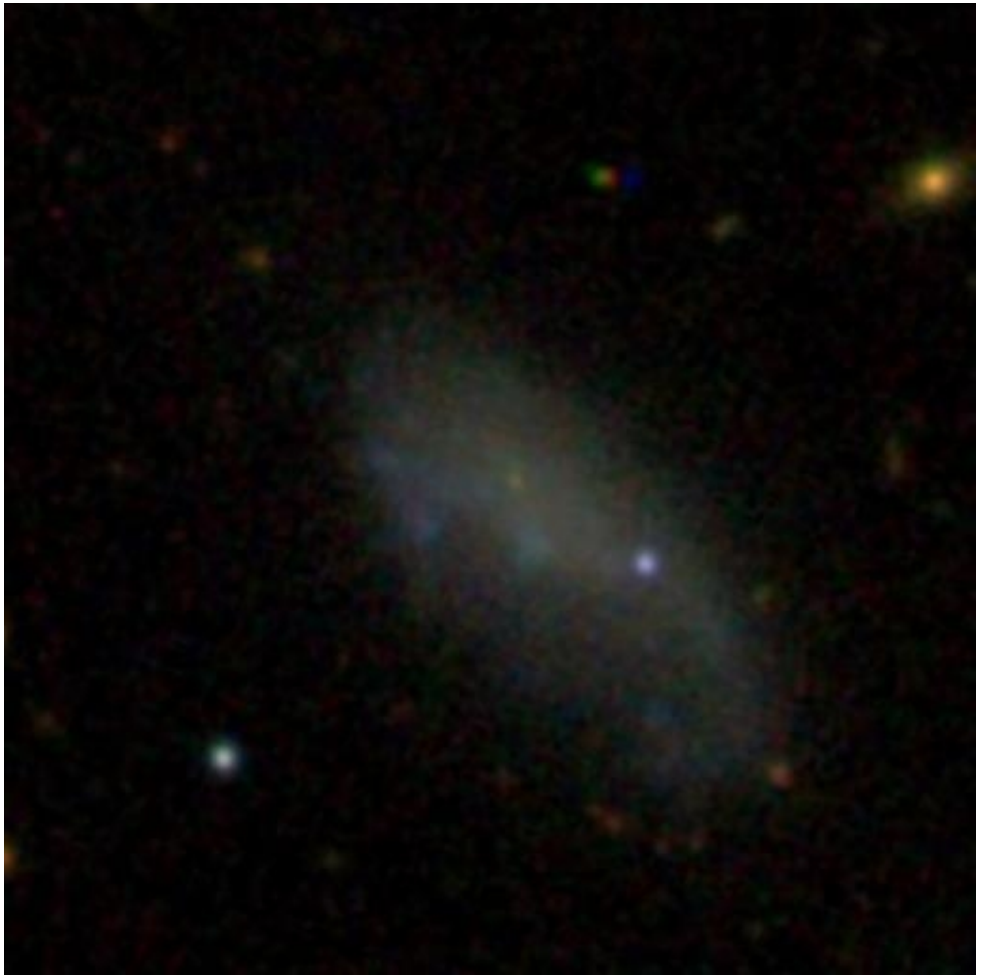

Table 1. Parameters for QSO-galaxy pair

		Note
Properties of UGC 5282		
RA, Dec (J2000):	09:51:10.03, +33:07:48.5	1
Heliocentric velocity $v_\odot$:	1577 ± 3 km s^{-1}	2
Adopted Distance D:	22.0 ± 0.2 Mpc	3
SDSS mag g, M_g, $g-r$:	15.5, −16.3, 0.42	4
Johnson mag B, M_B, L:	15.7, −16.0, $0.02L_*$	5
Radius $R_{25}(r)$:	$34'' \equiv 3.7$ kpc	6
$\mu_c(r)$:	21.7 mags arcsec^{-2}	6
H I mass [log($M_\odot$)]:	$\simeq 8.5$	7
Star Formation Rate:	$0.05-0.1\,M_\odot$ yr^{-1}	8
Stellar mass [log($M_\odot$)]:	8.5 ± 0.2	9
Specific SFR [log(yr^{-1})]:	-9.5 ± 0.2	8
Halo mass log[$M_{200}(M_\odot)$]:	≈ 10.7	10
Properties of background QSO		
RA, DEC:	09:51:09.12 +33:07:45.8	11
Redshift:	0.644	11
Impact parameter ρ:	$11.7'' \equiv 1.2$ kpc	12

… с просвечивающим квазаром!

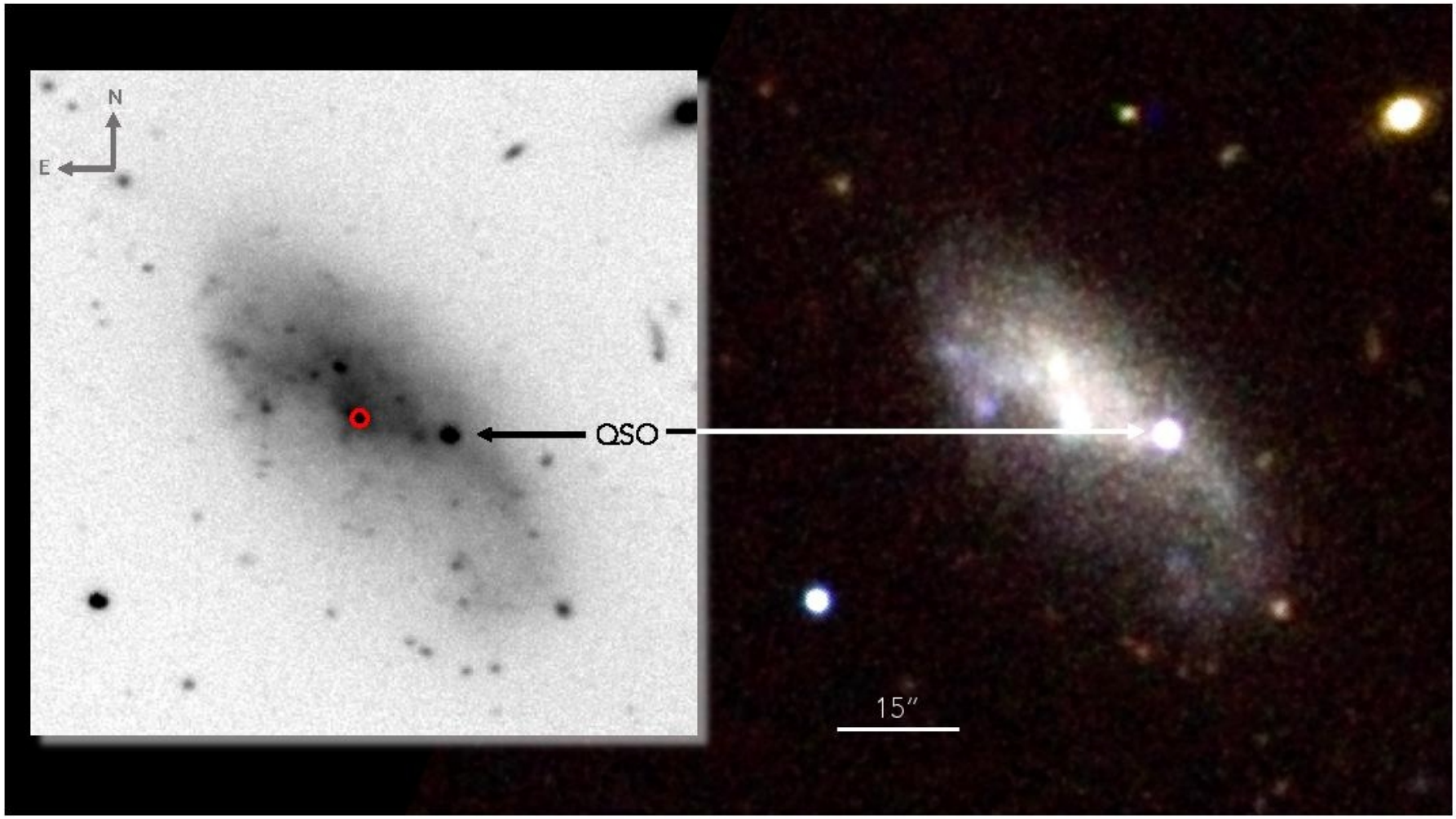

В группе, в паре с карликом, но еще в 250 кпк от большой спирали

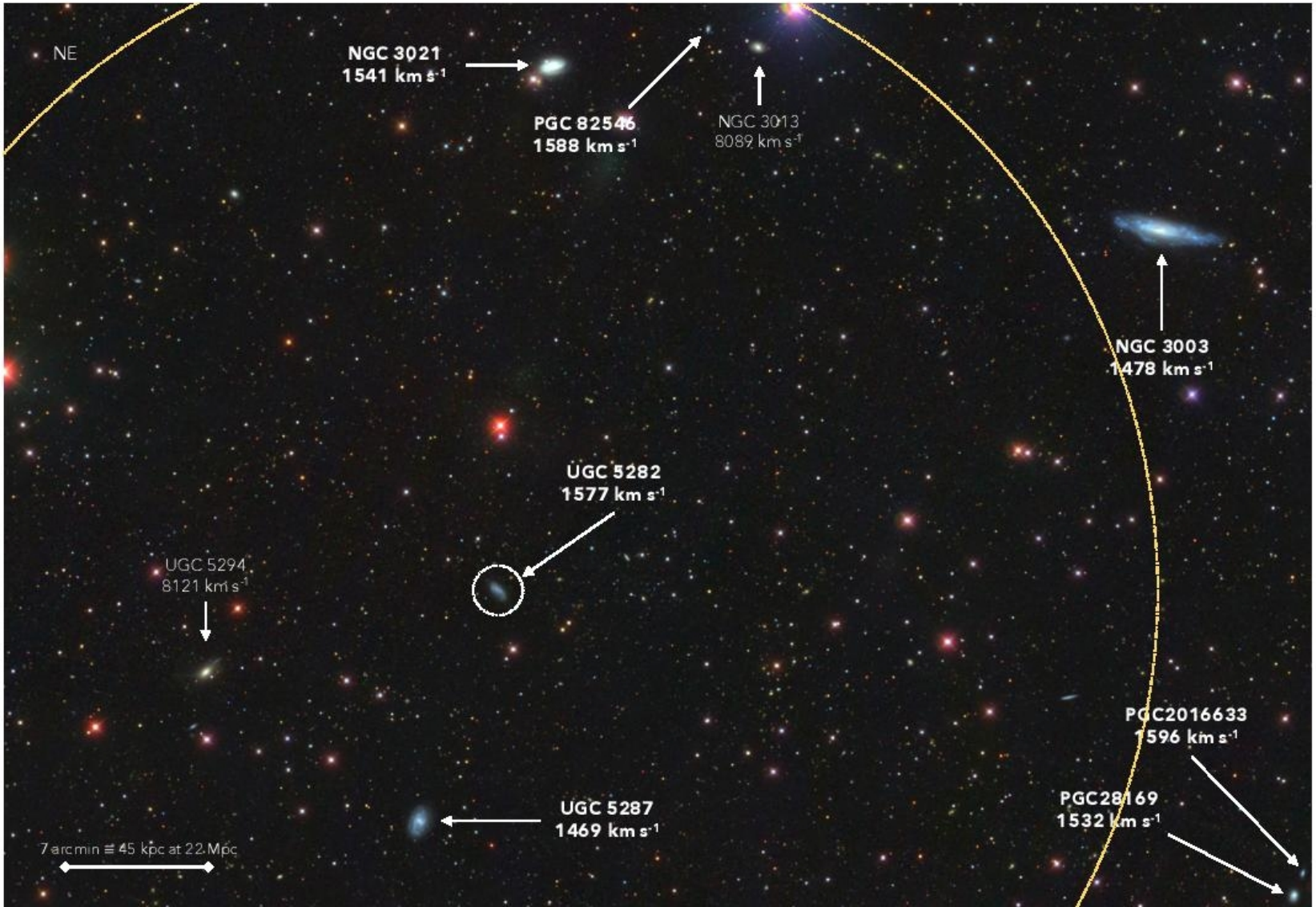

Металличность HII-области

Table 2. Strong Line Diagnostics of The Central H II Region of UGC 5282

Method ID	Method Line Ratios	Method σ_{SL} [a]	12 + log(O/H)	$Z_{H\,II}$ [b]	Calibration Ref.
Ar3O3	[Ar III] λ7135 / [O III] λ5007	±0.23	8.43 ± 0.10	–0.33 ± 0.11	1
S3O3	[S III] λ9069 / [O III] λ5007	±0.25	8.42 ± 0.03	–0.34 ± 0.06	1
S23	([S II] $\lambda\lambda$6716,6730 + [S III] $\lambda\lambda$9069,9530)/Hβ	±0.10	8.39 ± 0.03	–0.37 ± 0.06	2
N2	[N II] λ6583 / Hα	±0.16	8.26 ± 0.01	–0.50 ± 0.05	3
O3N2	([O III] λ5007 x Hα) / ([N II] λ6583 x Hβ)	±0.18	8.27 ± 0.01	–0.49 ± 0.05	3
KK04	f([O II] λ3727, [O III] λ4959,5007, Hβ, q)	±0.2	8.36	–0.40	4

[a] This is the the approximate 1σ dispersion in the calibration of the emission line ratio metallicities.

[b] Metallicity of the central H II region in UGC 5282, log(O/H) − log(O/H)$_\odot$ where 12+log(O/H)$_\odot$ = 8.76 (Lodders 2003). The errors listed in this column are only combined errors from the flux measurements.

References—1 — Stasinska (2006); 2 — Pérez-Montero & Díaz (2005); 3 — Marino et al. (2013); 4 — Kobulnicky & Kewley (2004)

И DLA-система в спектре квазара на красном смещении UGC 5282

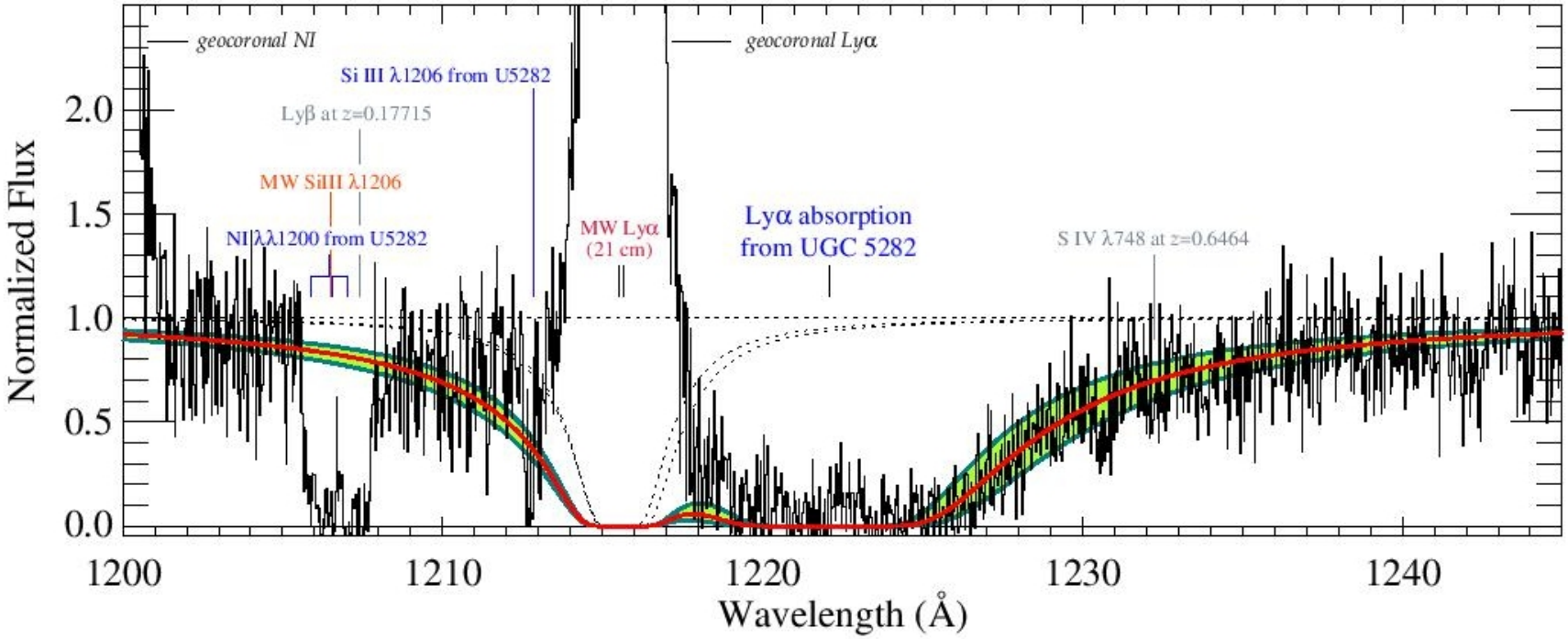

Figure 4. Normalized COS spectrum of the QSO J0951+3307. A composite Lyα absorption line profile is shown as a red line, which is comprised of absorption from UGC 5282 at $v = 1581$ km s^{-1} with $\log N(\mathrm{H\ I}) = 20.89$ (+0.12, –0.21), and two components inferred from 21 cm emission line measurements (black dotted lines) at –35 and 0 km s^{-1} with $\log N(\mathrm{H\ I}) = 19.79$ and 19.70, respectively. The region shown in green corresponds to profile fits made to data normalized by continuum fits that are 1σ deviant from the best fit continuum. The geocoronal emission lines from Lyα and N I are marked, as well as the wavelengths of other detected absorption lines.

Вот такой у нее хим. состав

Table 3. Results from Voigt Profile Fits to Weak Absorption Lines from UGC 5282

Ion (X)	Detected[a] Lines	$v = 1581 \pm 3$ km s^{-1} b (km s^{-1})	log[N(cm^{-2})]	N(X)/N(H I) − $Z_\odot$
H I	**λ1216**	...	20.89 (+0.12,–0.21)	...
	Lines fitted simultaneously to give single b and v values			
S II	λ1250, **λ1259**	15.5 ± 5.9	15.33 (+0.37, –0.15)	–0.82 (+0.39, –0.26)
P II	**λ1152**	15.5 ± 5.9	13.65 (+0.27, –0.24)	–0.78 (+0.30, –0.32)
Fe II	**λ1143**, λ1144, (**λ1142**)[b]	15.5 ± 5.9	15.02 (+0.33, –0.22)	–1.41 (+0.35, –0.31)
C II*	**λ1335**	15.5 ± 5.9	13.86 (+0.27, –0.25)	...
	Lines fitted assuming fixed b and/or v			
O I	**λ1302**	15.5	16.51 (+0.49, –0.72)	–1.14 (+0.51, –0.75)
		29.8 ± 17.7[c]	15.15 (+0.55, –0.32)	..
Si II	**λ1190**, **λ1304**	15.5	14.83±0.36	–1.67 (+0.38, –0.42)
		30.0 ± 6.2[c]	14.60 (+0.19, –0.12)	...

[a] Lines in bold indicate which lines were fit with Voigt profiles;

[b] Fe II λ1142 not detected, but data used to constrain fit;

[c] Additional component at $v = 1562$ km s^{-1}.

Металличность ниже, чем в HII-области!

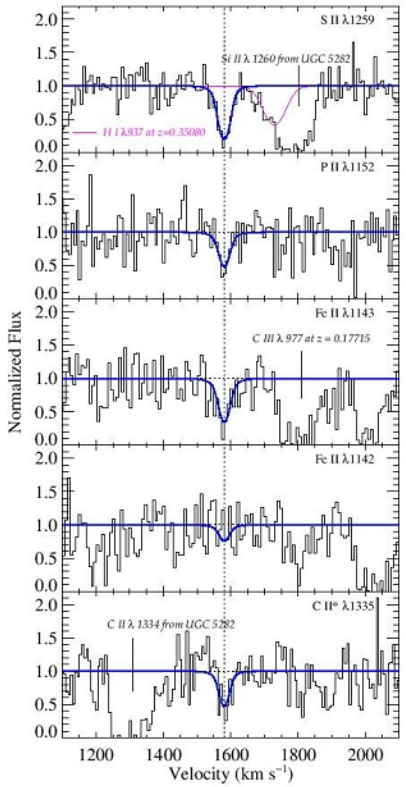

Figure 5. Sections of the normalized COS spectrum of J0951+3307 featuring the set of relatively weak absorption lines from different

The metallicities of S and P derived are sufficiently similar within their errors that we can take a simple weighted average of the two values to give a final estimate of the metallicity:

$$Z_{\rm H\,I}({\rm S,P}) \simeq -0.80 \pm 0.24\,.$$

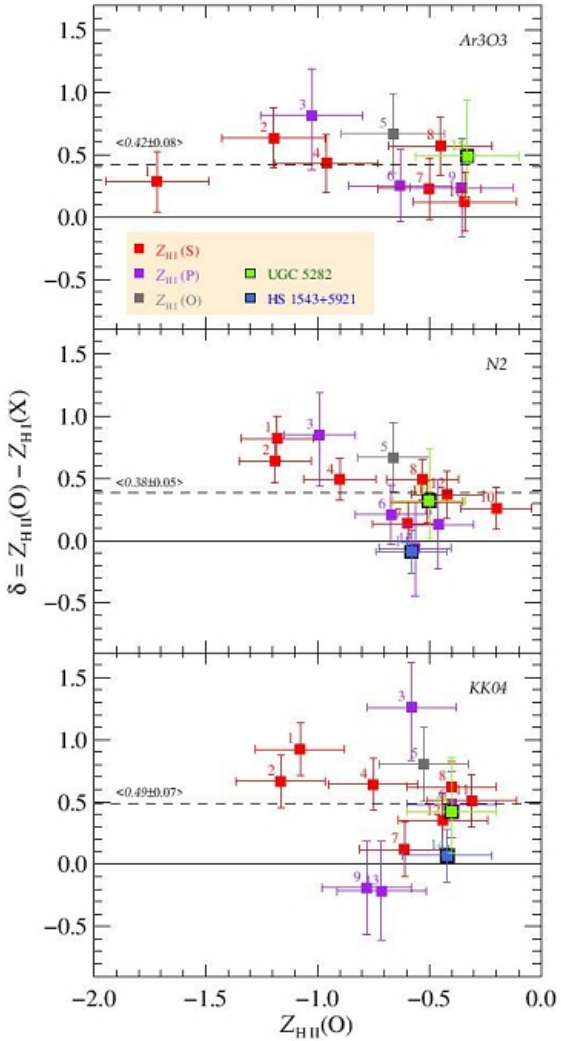

Figure 8. Plots showing the difference in metallicities δ between ionized gas ($Z_{\rm H\,II}$) measured from emission lines from H II regions, and neutral gas ($Z_{\rm H\,I}$) measured by absorption lines towards the H II

Надо ли поправить зависимость ‘масса-металличность’ ?

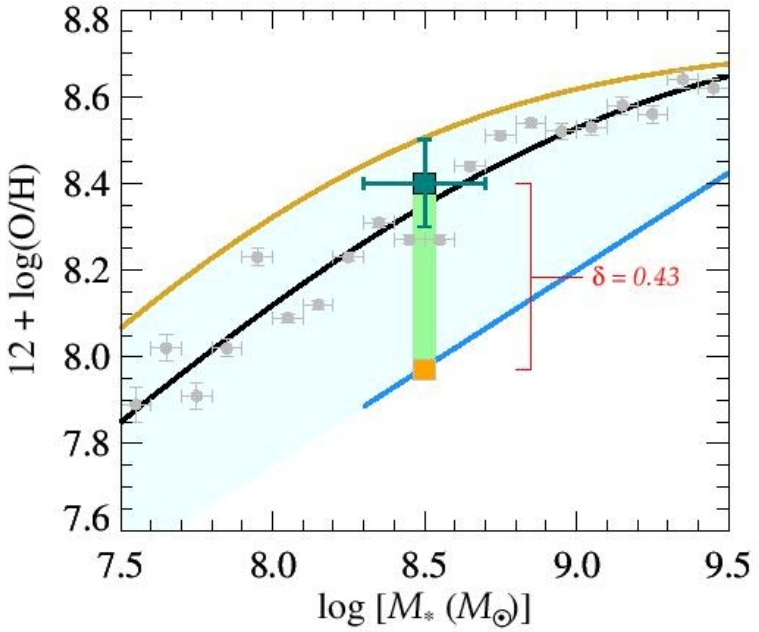

Figure 9. Comparison of the metallicity $Z_{\rm H\,II}$ and stellar mass of UGC 5282, to the stellar mass-metallicity-SFR ($M_* - Z - $SFR) relationship for 200,000 SDSS galaxies studied by Andrews & Martini (2013). The black line represents the $M_* - Z - $SFR relation found without considering the SFR of the sample galaxies; the grey circles show the data used to produce the black line and are included to indicate the dispersion in the data. The yellow and blue lines show the resulting $M_* - Z - $SFR relations when the galaxies are binned into a sample with low SFRs, $-1.0 \leq \log(\mathrm{SFR}) < -0.5$, and with high SFRs, $0.5 \leq \log(\mathrm{SFR}) < 1.0$, respectively. The green square shows the position of $Z_{\rm H\,II}$ for UGC 5282, while the orange square shows the value of $Z_{\rm H\,I}$. The difference between the two, the value of δ dis-

ArXiv: 2003.10458

Spinning Bar and a Star-formation Inefficient Repertoire:
Turbulence in Hickson Compact Group NGC7674

DIANE M. SALIM,[1,2] KATHERINE ALATALO,[3,4,5] CHRISTOPH FEDERRATH,[1,2] BRENT GROVES,[1,2] AND LISA J. KEWLEY[1,2]

[1]*Research School of Astronomy and Astrophysics, Australian National University, Canberra, ACT 2611, Australia*
[2]*ARC Centre Of Excellence For All Sky Astrophysics in 3D (ASTRO3D), Australia*
[3]*Space Telescope Science Institute, 3700 San Martin Dr., Baltimore, MD 21218, USA*
[4]*The Observatories of the Carnegie Institution for Science, 813 Santa Barbara St., Pasadena, CA 91101, USA*
[5]*Johns Hopkins University, Department of Physics and Astronomy, Baltimore, MD 21218, USA*

ABSTRACT

The physics regulating star formation (SF) in Hickson Compact Groups (HCG) has thus far been difficult to describe, due to their unique kinematic properties. In this study we expand upon previous works to devise a more physically meaningful SF relation able to better encompass the physics of these unique systems. We combine CO(1–0) data from the Combined Array from Research in Millimeter Astronomy (CARMA) to trace the column density of molecular gas $\Sigma_{\rm gas}$ and deep Hα imaging taken on the Southern Astrophysical Research (SOAR) Telescope tracing $\Sigma_{\rm SFR}$ to investigate star formation efficiency across face-on HCG, NGC7674. We find a lack of universality in star formation, with two distinct sequences present in the $\Sigma_{\rm gas} - \Sigma_{\rm SFR}$ plane; one for inside and one for outside the nucleus. We devise a SF relation based on the multi-freefall nature of gas and the critical density, which itself is dependent on the virial parameter $\alpha_{\rm vir}$, the ratio of turbulent to gravitational energy. We find that our modified SF relation fits the data and describes the physics of this system well with the introduction of a virial parameter of about 5–10 across the galaxy. This $\alpha_{\rm vir}$ leads to an order-of-magnitude reduction in SFR compared to $\alpha_{\rm vir} \approx 1$ systems.

NGC 7674, она же Arp182, Mrk 533, VV 343…

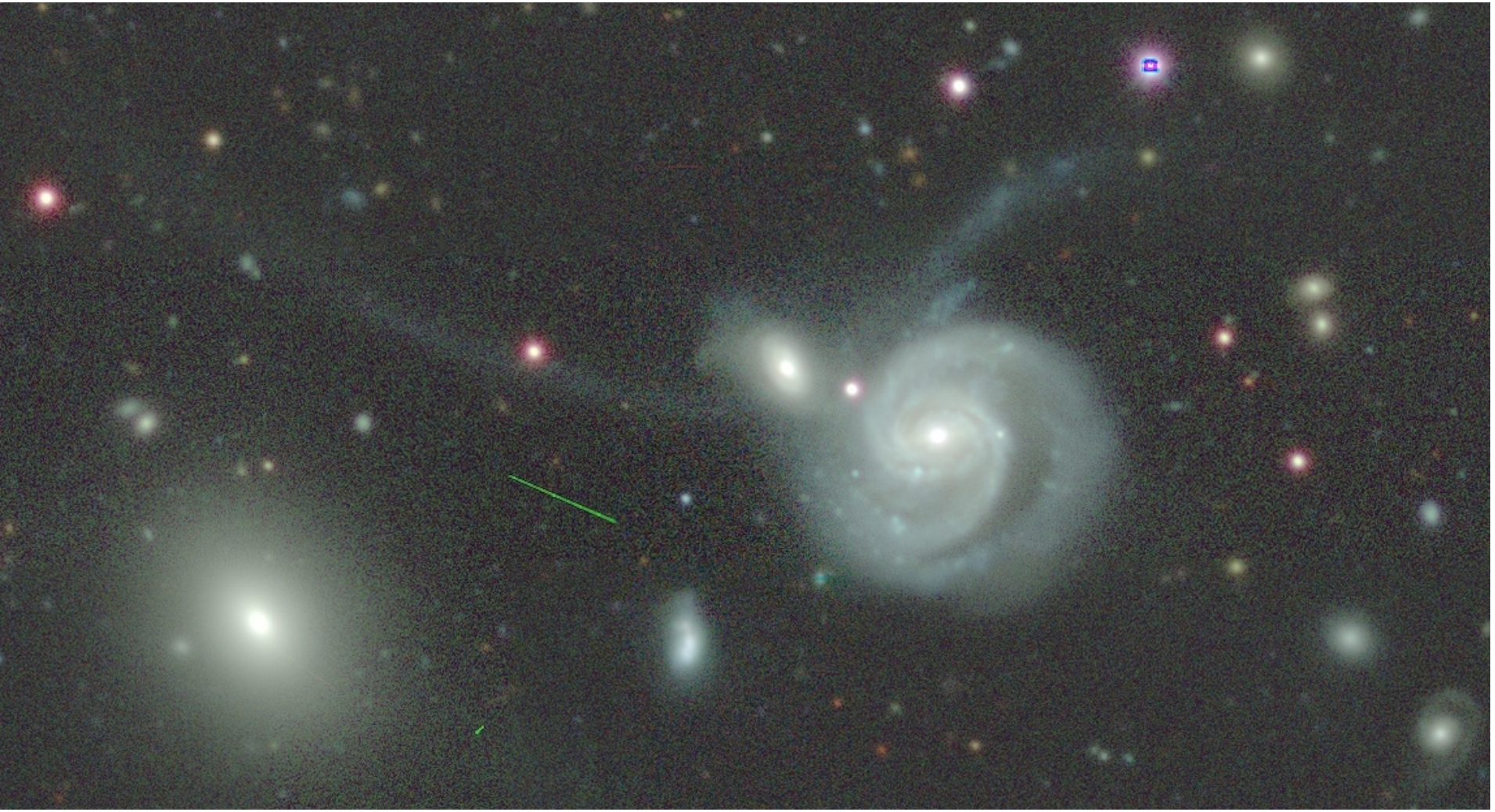

Картирование в CO и H-alpha

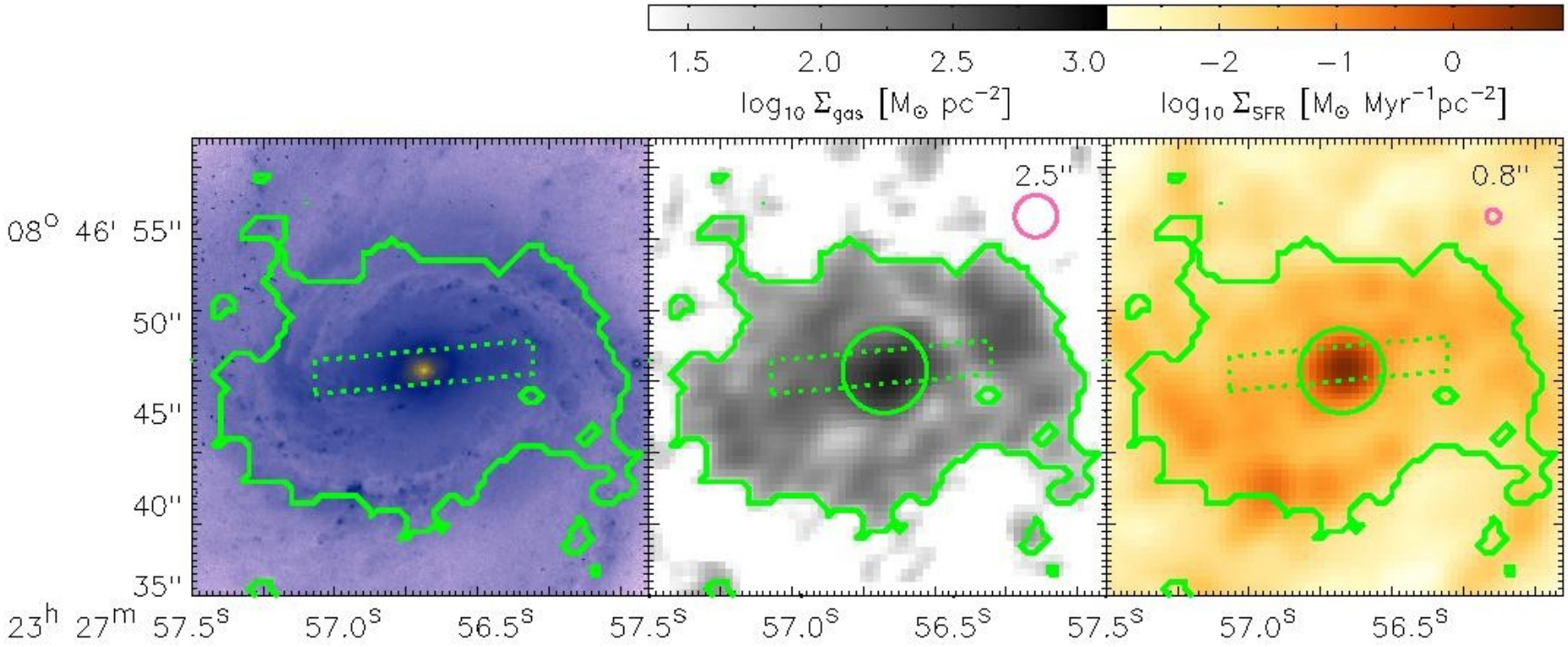

Figure 1. Hickson Compact Group NGC7674. *LEFT:* i-band image from the *Hubble Space Telescope (HST)* (Armus et al. 2009). *MIDDLE:* $\Sigma_{\rm gas}$ maps inferred from the CARMA CO(1-0) observations (Alatalo et al. 2015a). *RIGHT:* $\Sigma_{\rm SFR}$ maps inferred from deep Hα imaging taken with the 4.1m SOAR telescope. (Eigenthaler et al. 2015). In every panel, the outermost contour indicates the boundary at which we seperate the noise-dominated pixels to the signal-dominated pixels we use in analysis. The dotted green rectangle indicates the boundary of the bar of NGC7674, as visually determined by the HST i-band image. In the middle and right panels, the central green circle represents the boundary of the central nucleus, as determined by the deep Hα imaging. In the middle and right panels, the top-right pink circle indicates the FWHM of the beam of the instruments which took the observations. The FHWM of each respective instrument is written above the beam size.

Что-то не то с законом Кенникута-Шмидта: разброс и излом

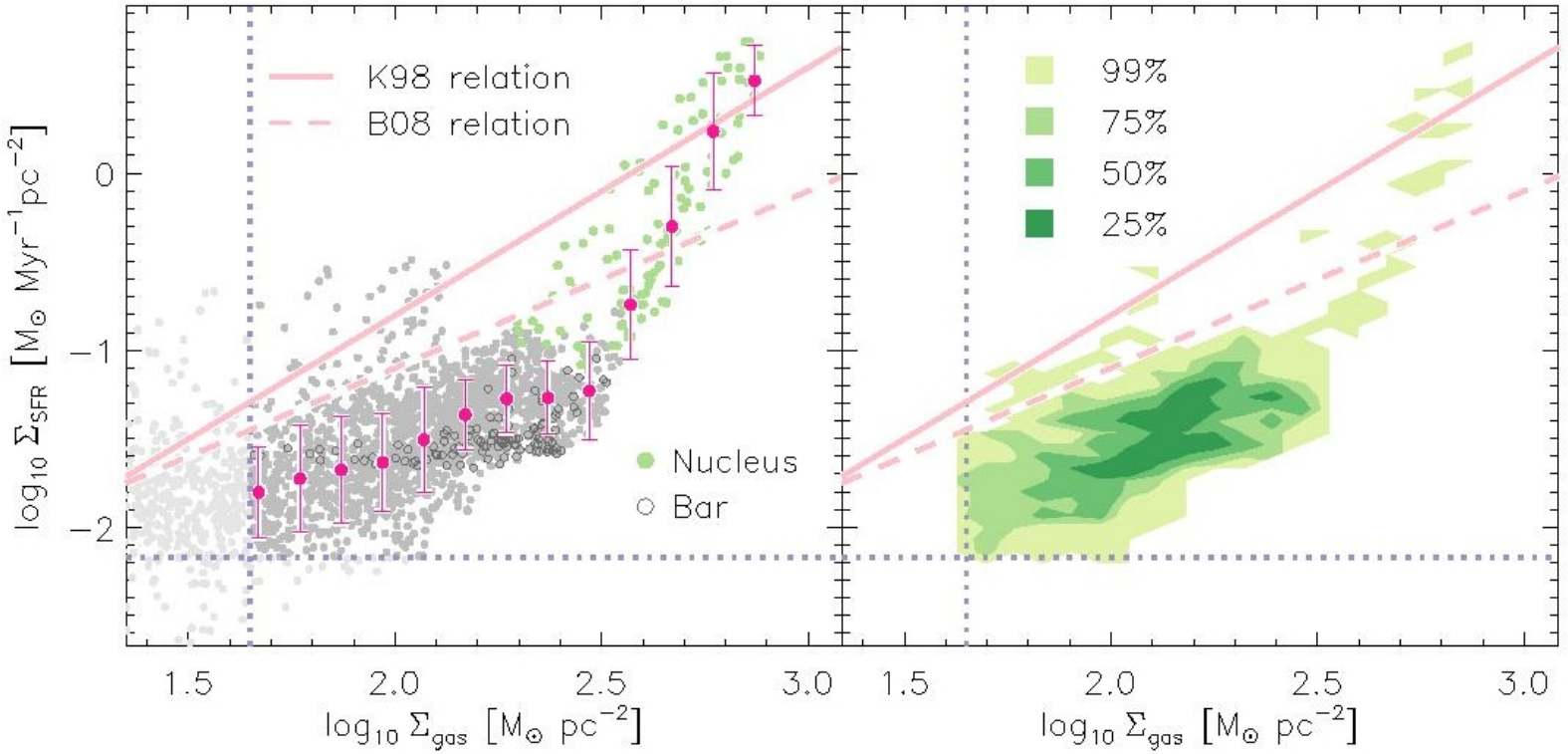

Figure 2. *LEFT:* We show the molecular gas surface density from CO(1–0) of every line of sight column in NGC7674's CARMA field compared to the Σ_{SFR} for the same column. Each LOS column is represented as a single circular data point in the left panel of the diagram. Green circles indicate pixels that fall within the bounds of the galactic nucleus and outlined circles highlight pixels that make up the bar outside the nucleus (see Fig. 1 for the parts of the galaxy defined as nucleus and bar, respectively). Both of these regions are defined in Section 2.4. The overlaid dark pink circles are the median Σ_{SFR} within Σ_{gas} bins of 0.1 dex of $M_\odot pc^{-1}$. The vertical error bars extending above and below these points are the standard deviations of Σ_{SFR} within each Σ_{gas} bin. The Kennicutt (1998) (K98) and Bigiel et al. (2008) (B08 hereafter) relations are also displayed on the same axes as the solid and dashed pink lines respectively. The lower thresholds in Σ_{gas} and Σ_{SFR}, as described in Section 2.4, are also shown in Figure 2 as the dotted purple vertical and horizontal dashed lines respectively. Any values in either Σ_{gas} or Σ_{SFR} that are lower than these thresholds we disregard and show in a fainter gray. Note that because the pixel size of the CARMA grid

Времена исчерпания HE коррелируют с плотностью газа

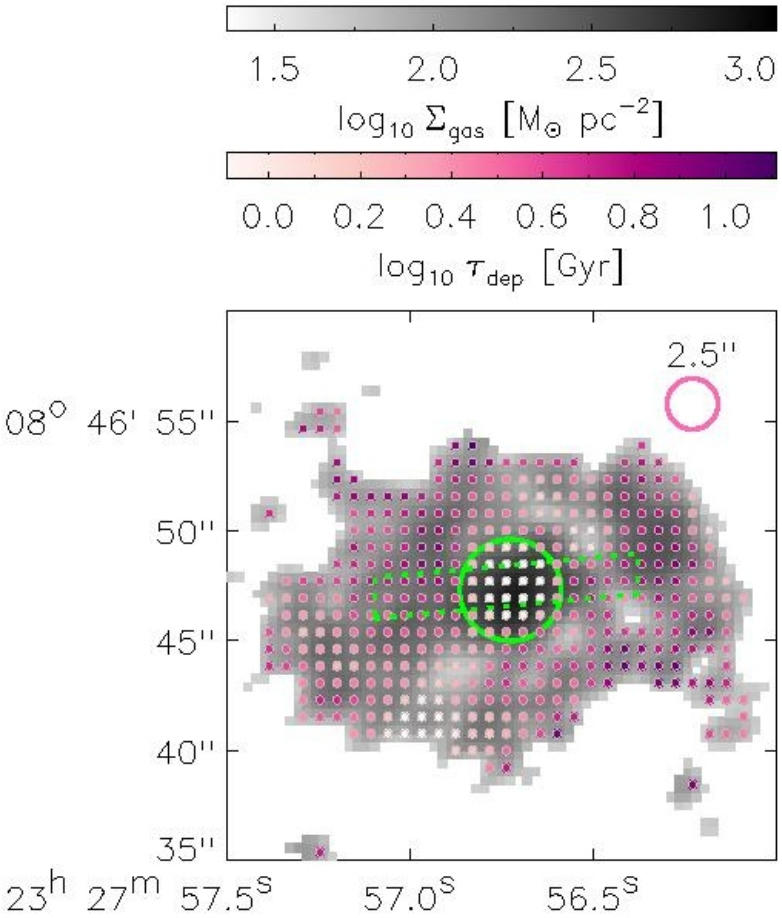

Figure 3. Average depletion time (pink colour gradient) of every 2×2 line of sight columns overlaid on top of the corresponding $\Sigma_{\rm gas}$ map (grayscale). Only pixels above the $\Sigma_{\rm gas}$ and $\Sigma_{\rm SFR}$ noise thresholds are shown.

Надо учесть турбулентность газа!

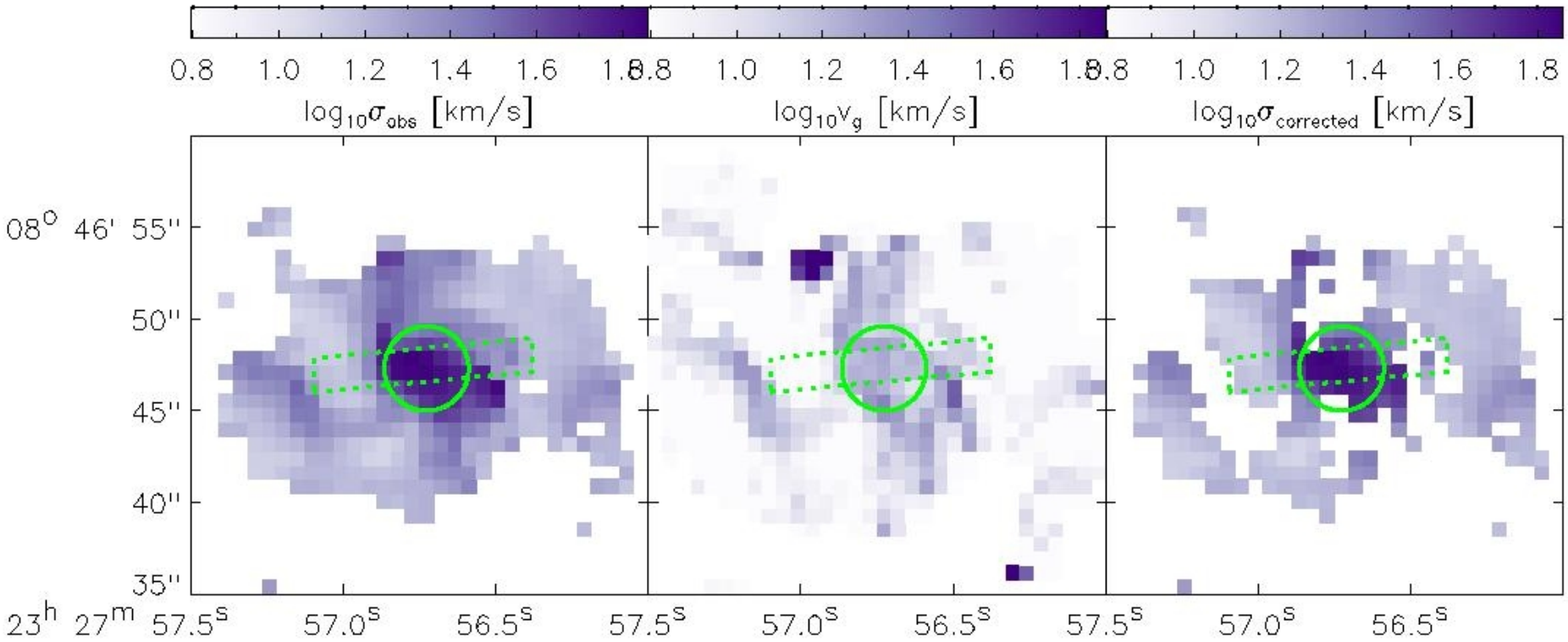

Figure 5. *LEFT PANELS:* The uncorrected velocity dispersion (moment2) map, the values of which are derived from the standard deviation of the Gaussian for each spectrum shown in Figure 4. *MIDDLE PANELS:* Velocity gradients across the galaxy. *BOTTOM PANELS:* The gradient-corrected velocity dispersions of the galaxy (velocity gradient subtracted from fitted Gaussian standard deviations.)

Три закона SF vs плотность газа

the Kennicutt (1998) (hereafter K98) SF power-law relation:

$$\Sigma_{\rm SFR} \propto \Sigma_{\rm gas}^{1.4} \tag{1}$$

and the Krumholz et al. (2012) (hereafter KDM12) relation, which correlate $\Sigma_{\rm SFR}$ to the ratio between the mean column gas density and the mean free-fall time $t_{\rm ff}(\rho_0)$ of the cloud, which is the time scale required for a medium with negligible pressure support to collapse. By doing so, the self-gravity of the system is taken into account:

$$\Sigma_{\rm SFR} = \epsilon_{\rm ff} \frac{\Sigma_{\rm gas}(\rho_0)}{t_{\rm ff}(\rho_0)} \,, \tag{2}$$

пусть магнитного поля нет!

The SFK15 relation uses the fact that $\Sigma_{\rm gas}$ and the density ρ closely follow a log-normal probability density function (PDF) in both simulations and observations (Krumholz et al. 2012; Federrath 2013a):

$$p(s)ds = \frac{1}{\sqrt{2\pi\sigma_s^2}} \exp\Big(-\frac{(s-s_0)^2}{2\sigma_s^2}\Big)ds, \tag{15}$$

where the density variable s is expressed as the logarithm of the density normalized to the mean density:

$$s = \ln(\rho/\rho_0) \tag{16}$$

and the logarithmic density variance σ_s is defined as derived by Padoan & Nordlund (2011) and Molina et al. (2012):

$$\sigma_s^2 = \ln\Big(1 + b^2\mathcal{M}^2\frac{\beta}{\beta+1}\Big). \tag{17}$$

σ_s^2 is itself parameterised by the turbulence driving parameter b, which represents the degree of compressive or solenoidal turbulence in the system (Federrath et al. 2008, 2010), the sonic Mach number $\mathcal{M}$, and the ratio between thermal and magnetic pressure β. SFK15 then derived their SF correlator by integrating over all densities for the entire PDF. The new correlator is denoted as the *maximum* or *multi-freefall gas consumption rate*, $(\Sigma_{\rm gas}/t)_{\rm multi-ff}$:

$$\Big(\frac{\Sigma_{\rm gas}}{t}\Big)_{\substack{\rm multi-ff\\ \rm SFK15}} = \frac{\Sigma_{\rm gas}(\rho_0)}{t_{\rm ff}(\rho_0)} \int_{-\infty}^{\infty} \exp\Big(\frac{3}{2}\,s\Big)\, p(s)\, ds\,. \tag{18}$$

By computing the integral and calibrating to Milky Way (MW) clouds and the Small Magellanic Cloud (SMC), the SFK15 model is reduced to:

$$\Sigma_{\rm SFR} = 0.45\% \times \Big(\frac{\Sigma_{\rm gas}}{t}\Big)_{\substack{\rm multi-ff\\ \rm SFK15}} \tag{19}$$

$$= 0.45\% \times \frac{\Sigma_{\rm gas}(\rho_0)}{t_{\rm ff}(\rho_0)} \times \Big(1 + b^2\mathcal{M}^2\frac{\beta}{\beta+1}\Big)^{3/8}. \tag{20}$$

SFK15 had assumed a natural mixed turbulence scenario

b=0.3

Сравнение предсказаний 3х законов звездообразования

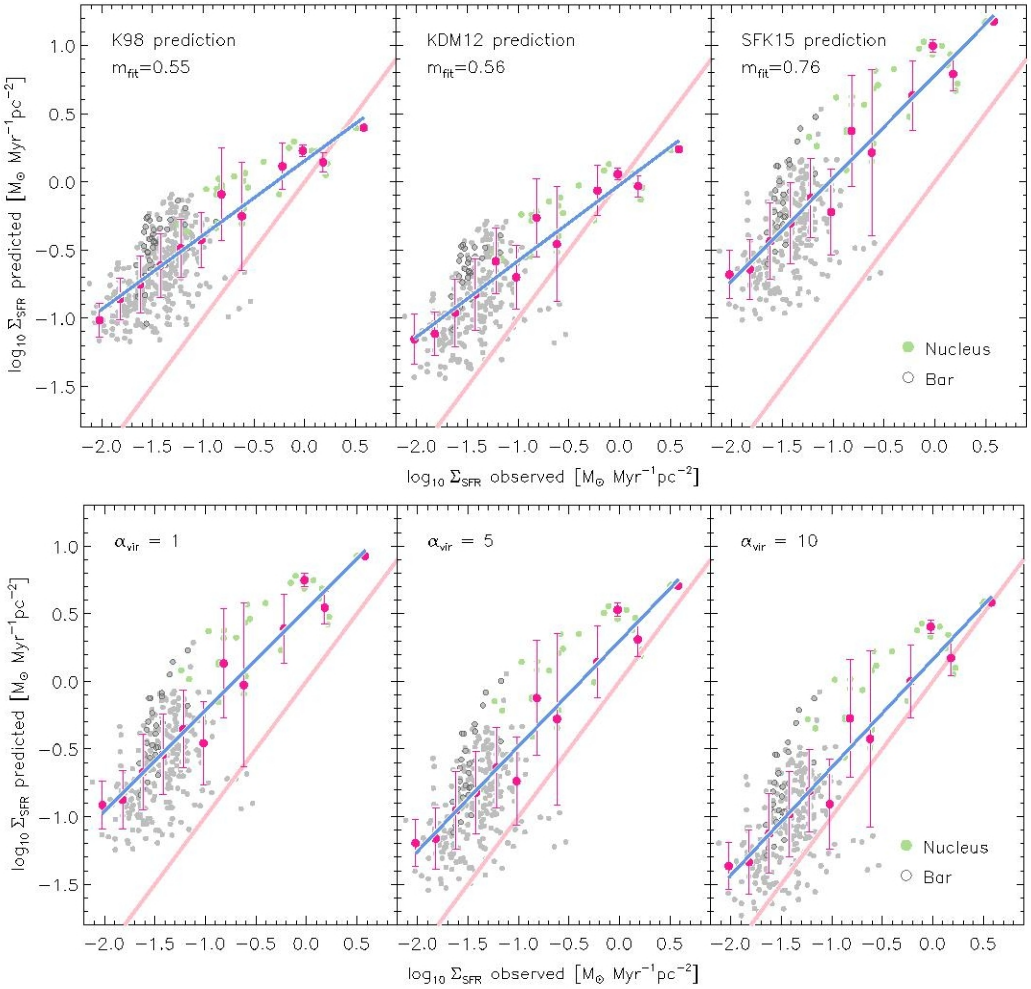

Figure 7. Same as the right-hand panel of Fig. 6, but for the extended comparison between Σ_{SFR} predicted using this work's extended turbulence-regulated SF model (Equation 26) for assumed α_{vir} of 1, 5 and 10 to the observed Σ_{SFR} inferred from deep Hα imaging. The resultant slopes and offsets between the predicted and observed Σ_{SFR} for each of the α_{vir} = 1, 5 and 10 scenarios for this SF model are tabulated in Table 1.

- Три вышеупомянутых закона
- А тут еще и порог по плотности, ~ вириальному коэффициенту

То же самое в таблице

SF prediction.	Offset	Slope
K98	0.15	0.55
KDM12	-0.02	0.56
SFK15	0.78	0.76
This work, $\alpha_{\rm vir} = 1$	0.54	0.75
This work, $\alpha_{\rm vir} = 5$	0.30	0.78
This work, $\alpha_{\rm vir} = 10$	0.16	0.80

Table 1. The offset and slope of the best least-squares linear fit to the median predicted $\Sigma_{\rm SFR}$ values within each observed $\Sigma_{\rm SFR}$ bin for the three previously derived SF models by K98, KDM12 and SFK15, as well as the extended turbulence-regulated SF relation derived in this work, for assumed $\alpha_{\rm vir}$ of 1, 5 and 10. A perfect correlation between predicted and observed $\Sigma_{\rm SFR}$ would result in an offset of 0 and a slope of 1.